

Metformin-induced reductions in tumor growth involves modulation of the gut microbiome*



Lindsay A. Broadfield^{1,2}, Amna Saigal¹, Jake C. Szamosi^{3,5}, Joanne A. Hammill⁴, Ksenia Bezverbnaya⁴, Dongdong Wang^{1,2}, Jaya Gautam^{1,2}, Evangelia E. Tsakiridis^{1,2}, Fiorella Di Pastena^{1,2}, Jamie McNicol⁴, Jianhan Wu^{1,2}, Saad Syed^{1,2,3}, James S.V. Lally^{1,2}, Amogelang R. Raphenya⁵, Marie-Jose Blouin^{7,8}, Michael Pollak^{7,8}, Andrea Sacconi⁹, Giovanni Blandino⁹, Andrew G. McArthur^{1,5}, Jonathan D. Schertzer^{1,3,5}, Michael G. Surette^{1,2,3,5}, Stephen M. Collins^{2,3}, Jonathan L. Bramson⁴, Paola Muti^{1,6}, Theodoros Tsakiridis^{1,6}, Gregory R. Steinberg^{1,2,5,*}

ABSTRACT

Background/Purpose: Type 2 diabetes and obesity increase the risk of developing colorectal cancer. Metformin may reduce colorectal cancer but the mechanisms mediating this effect remain unclear. In mice and humans, a high-fat diet (HFD), obesity and metformin are known to alter the gut microbiome but whether this is important for influencing tumor growth is not known.

Methods: Mice with syngeneic MC38 colon adenocarcinomas were treated with metformin or feces obtained from control or metformin treated mice.

Results: We find that compared to chow-fed controls, tumor growth is increased when mice are fed a HFD and that this acceleration of tumor growth can be partially recapitulated through transfer of the fecal microbiome or *in vitro* treatment of cells with fecal filtrates from HFD-fed animals. Treatment of HFD-fed mice with orally ingested, but not intraperitoneally injected, metformin suppresses tumor growth and increases the expression of short-chain fatty acid (SCFA)-producing microbes *Alistipes*, *Lachnospiraceae* and *Ruminococcaceae*. The transfer of the gut microbiome from mice treated orally with metformin to drug naïve, conventionalized HFD-fed mice increases circulating propionate and butyrate, reduces tumor proliferation, and suppresses the expression of sterol response element binding protein (SREBP) gene targets in the tumor.

Conclusion: These data indicate that in obese mice fed a HFD, metformin reduces tumor burden through changes in the gut microbiome.

© 2022 The Author(s). Published by Elsevier GmbH. This is an open access article under the CC BY-NC-ND license (<http://creativecommons.org/licenses/by-nc-nd/4.0/>).

Keywords Gut microbiome; Metformin; High-fat diet; Obesity; Colon cancer

1. INTRODUCTION

Obesity and type 2 diabetes are important risk factors for many cancers including colorectal cancer [1,2]. Type 2 diabetes increases the risk of developing CRC by 27% [3], and this elevated risk has been found to be independent of type 2 diabetes duration [4]. While type 2 diabetes and CRC share a number of risk factors, including age, obesity, smoking, and alcohol consumption, a definitive biological link between the development of these two diseases has not been identified. Rather, numerous biological mechanisms have been proposed, including elevations in circulating glucose and insulin, adipokines and chemokines, and immune function [5]. With the overlapping risk factors that can lead to either disease, and increased CRC risk with type 2 diabetes, understanding how

therapies traditionally used for type 2 diabetes treatment present an opportunity for CRC prevention.

Metformin is a first-line therapy for type 2 diabetes and may have preventative effects against some cancers including CRC; a concept being tested in several clinical trials [6,7]. Mechanisms for the anti-tumor effects of metformin have been widely studied but can be summarized to broadly involve either direct or indirect effects (reviewed in [8,9]). Direct effects include metformin entering the tumor and altering tumor metabolism and associated signaling cascades while indirect, effects may involve reductions in circulating metabolic substrates and growth factors such as glucose and insulin which support and sustain tumor cell proliferation (reviewed in [8,9]). In support of an indirect mechanism of action for metformin, clinical concentrations of metformin appear to have little effect on tumor

***One Sentence Summary:** Metformin-induced changes in the gut microbiome are important for suppressing the growth of syngeneic colorectal cancer cells in obese, insulin resistant mice fed a high-fat diet.

¹Centre for Metabolism, Obesity and Diabetes Research, McMaster University, Hamilton, ON, Canada ²Department of Medicine, McMaster University, Hamilton, ON, Canada ³Farncombe Family Digestive Research Institute, McMaster University, Hamilton, ON, Canada ⁴Department of Pathology and Molecular Medicine, McMaster University, Hamilton, ON, Canada ⁵Department of Biochemistry and Biomedical Sciences, McMaster University, Hamilton, ON, Canada ⁶Department of Oncology, McMaster University, Hamilton, ON, Canada ⁷Segal Cancer Center, Lady Davis Institute for Medical Research, Jewish General Hospital ⁸Gerald Bronfman Department of Oncology, McGill University, Montreal, Canada ⁹Oncogenomic and Epigenetic Unit, Italian National Cancer Institute "Regina Elena", Rome, Italy

*Corresponding author. HSC 4N63, 1280 Main St W, Hamilton, ON, Canada, L8S 4K1. E-mail: gsteinberg@mcmaster.ca (G.R. Steinberg).

Received January 6, 2022 • Revision received February 25, 2022 • Accepted April 11, 2022 • Available online 20 April 2022

<https://doi.org/10.1016/j.molmet.2022.101498>

Abbreviations:

AUC	area under the curve
CRC	colorectal cancer
FMT	fecal microbiome transfer
GMB	gut microbiome
HFD	high-fat diet
HMGCR	HMG-CoA reductase
OTU	operational taxonomic unit
SCFA	short-chain fatty acid
SPF	specific pathogen free
SREBP	sterol response element binding protein

growth *in vitro* and in pre-clinical mouse models where metformin suppresses CRC growth most notably in obese insulin resistant mice that are fed a high-fat diet (HFD) [10–12]. These data suggest that metformin-suppresses tumor growth through indirect mechanisms, however, the mechanisms mediating these effects remain undefined. The development of both CRC and type 2 diabetes have been linked to changes in the diversity of the gut microbiome (GMB) [13–16] and subsequent production of short-chain fatty acids (SCFA) [17–19]. Specifically, a diet high in fiber has been shown to increase butyrate production and reduce CRC while a HFD reduces butyrate and may increase CRC proliferation (reviewed in [20]). Changes in the GMB and increases in SCFAs have also been linked to the glucose lowering effects of metformin in rodent models and humans [21–24]. However, whether metformin-induced changes in the GMB and SCFA are important for suppressing CRC is not currently known. In the current study we have examined whether metformin-modulation of the GMB is important for eliciting changes in CRC growth and what potential mechanisms may be involved. We find, using a variety of *in vitro* and *in vivo* approaches, that metformin induced increases in butyrate-producing gut microbes are important for reducing tumor growth in mice fed a HFD.

2. RESULTS

2.1. High-fat diet feeding induced changes in the gut microbiome promote tumor growth

In order to investigate the interactions between diet and tumor growth we conducted experiments in obesity and insulin resistance prone male C57BL/6J mice grafted with carcinogen-induced syngeneic murine colon cancer cells (MC38) established from the C57BL/6 mouse line. MC38 cells were subcutaneously injected after a 12-week long feeding protocol on standard chow diet (17% kcal fat) or high-fat diet (HFD, 45% kcal fat). Consistent with previous findings using this model system [10–12], HFD-fed mice had increased body mass, adiposity, fasting blood glucose, fasting serum insulin (Figs. S1A–D), and accelerated tumor growth compared to chow-fed controls (Figure 1A). To evaluate the role of the GMB in these effects, chow-fed recipient animals received fecal microbiome transfers (FMT) from control chow-fed donors (generating Chow–Chow FMT recipients) or HFD-fed donors (generating HFD–Chow FMT recipients) for 4 weeks prior to injection of MC38 cells. The FMT protocol continued throughout tumor growth (Figure 1B). Sequencing the v3 region of bacterial 16S rRNA of feces confirmed that β -diversity was distinct between chow and HFD donors. Further, the Chow–Chow–FMT recipients had overlapping β -diversity with their chow donors while the HFD–Chow–FMT had a distinctly different β -diversity (Figure 1C). Overall, diet accounted for 18.6% of all variation in β -diversity ($p < 0.001$). Direct

exposure to HFD (HFD donors) altered the relative abundance of bacteria at the phylum level, with a decreased *Bacteroidetes* and increased *Tenericutes* abundances (Figure 1D). In HFD–Chow FMT recipients, *Verrucomicrobia*, *Actinobacter*, and *Tenericutes* were followed a similar trend, with elevated levels of these phylum detected when compared to HFD donor mice (Figure 1C, Table S1). In HFD–Chow–FMT mice, the relative abundances at the phylum level were more similar to Chow-fed donors than the HFD-fed donors. Remarkably, there was a strong trend for accelerated tumor growth rates in the HFD–chow FMT mice (Figure 1E,F, AUC for tumor growth rate $p = 0.0549$). Importantly, this tendency for an increase in tumor growth rate with the HFD–fecal transplants was independent of any change in body mass, adiposity or circulating glucose, suggesting a potential direct effect of the GMB or its by-products (Figs. S1E–G). In order to directly examine the role of the GMB, we collected fecal pellets from chow and HFD-fed animals, homogenized the fecal pellets in growth medium, sterile filtered the homogenate, and used the extracted fecal filtrate to test its effects on MC38 proliferation. Interestingly, and consistent with our *in vivo* observations, we detected a small ($\sim 10\%$) but significant increase in MC38 cell proliferation when cultured in fecal filtrate (0.1%) from HFD-fed animals compared to chow-fed controls (Figure 1G). Together, these *in vitro* and *in vivo* data suggest that the HFD alters the production of bacterial derived metabolites that promote tumor growth, or that the chow diet produces metabolites that hinder tumor growth.

2.2. Oral but not intraperitoneal delivery of metformin to mice fed a HFD alters the GMB and suppresses tumor growth

Metformin changes the GMB [21,24,25], but whether this is important for inhibiting cancer growth is not known. To examine the importance of the GMB in metformin action, we first compared the effects of metformin method of delivery, testing for changes in tumor growth and GMB diversity and composition in mice treated with metformin through daily intraperitoneal (IP) injections compared to oral metformin delivery (via drinking water) in HFD-fed mice. We utilized distinct doses of metformin (100 mg/kg IP or 250 mg/kg drinking water) to elicit similar tumor concentrations of metformin [26,27] and hypothesized that oral but not intraperitoneal metformin delivery would elicit significant changes in GMB diversity and reductions in tumor growth rates. Intraperitoneal delivery of metformin had no effect on tumor growth (Figure 2A), while oral delivery of metformin in drinking water reduced tumor growth by $\sim 40\%$ (Figure 2B). Consistent with no change in tumor growth, intraperitoneal delivery of metformin had minimal effects on β -diversity, relative phyla abundance, body mass, fasting blood glucose, or serum insulin (Figs. S2A–E). In contrast, oral metformin delivery altered β -diversity (Figure 2C, causing 22.5% of variation, $p < 0.0001$), and we found it reduced the abundance of *Tenericutes* while increasing *Bacteroidetes*, *Verrucomicrobia*, and *Proteobacteria* (Figure 2D). Oral metformin delivery was also associated with reductions in body mass, and trends for reduced fasting blood glucose and serum insulin (Figure 2E–G). These data suggest a potentially important role of the GMB in mediating the effects on metformin on suppressing tumor growth, however, it should be noted these findings could also be due to multiple other mechanisms; such as differential exposure of the tumor to metformin [26,27], reductions in body weight or alterations in glucose, insulin or other hormonal factors.

2.3. Metformin-induced reductions in tumor growth can be recapitulated through fecal transplants of the microbiome

In order to more directly evaluate whether the GMB was mediating the effects of metformin on tumor growth, HFD-fed mice received a fecal

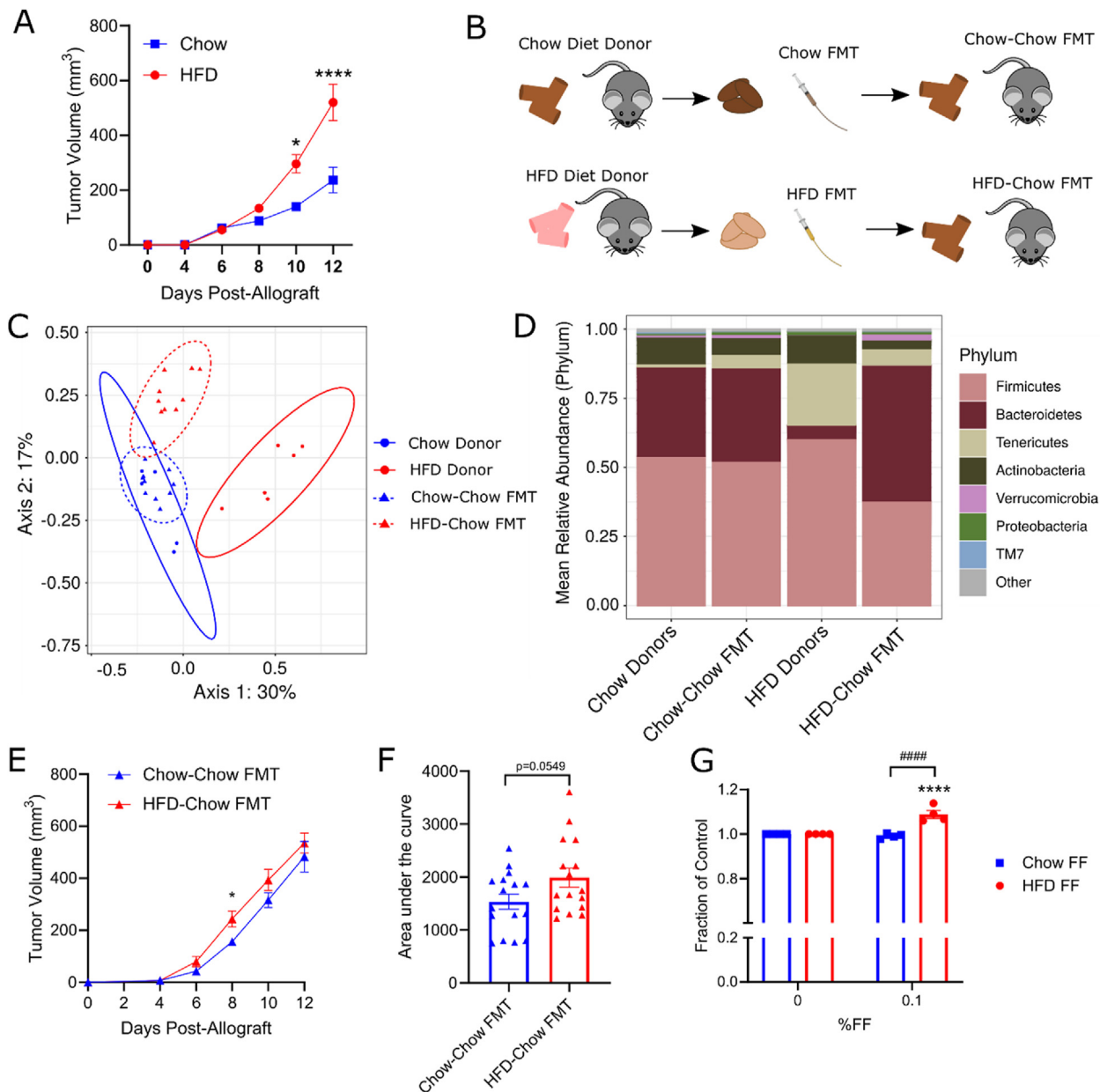


Figure 1: Feeding a high-fat diet (HFD) alters the gut microbiome and stimulates MC38 allograft growth. A) MC38 tumor volume in mice fed a standard chow ($n = 5$) or HFD ($n = 13$). B) Fecal microbiome transfer (FMT) protocol schematic. Donor and recipient mice were housed separately. 200 μ L of fecal homogenate from donor mice were orally delivered to recipient mice 3 times weekly. C) Principle coordinates of analysis of Bray–Curtis distances of 16S rRNA sequencing of fecal samples from chow ($n = 5$) and HFD-fed ($n = 6$) donors, and chow-fed chow (chow–chow FMT, $n = 10$) and HFD (HFD–Chow FMT, $n = 10$) FMT recipients. D) Average relative abundances of fecal GMB phylum in fecal donor (chow donor $n = 5$, HFD donor $n = 5$) and FMT recipient (Chow–Chow FMT $n = 10$, HFD–Chow FMT $n = 10$) animals. E) MC38 tumor allograft growth in Chow–Chow FMT ($n = 16$) and HFD–Chow FMT ($n = 16$) recipient animals. F) Tumor growth rate as calculated by the area under the curve (AUC) of the tumor growth curve ($n = 16$ per group). G) 72-hour MC38 in vitro cell proliferation with chow or HFD fecal filtrate (FF; $n = 4$ independent experiments per condition). **** indicates differences between 0% and 0.1% FF, ##### indicates differences between chow FF and HFD FF. Statistics: Unpaired two-sided t-testing (F), nonrepeated measures (G) and repeated measures (A, E) 2-way ANOVA were used to test for differences between diet groups and FMT treatments with Fisher LSD post-hoc testing. * $p < 0.05$, *** $p < 0.001$, **** $p < 0.0001$, ##### $p < 0.0001$.

microbiome transfer (FMT) from either HFD-control mice (generating HFD FMT mice) or HFD-metformin treated mice (generating HFD-Met FMT mice) (Figure 3A). The transfer of metformin-treated feces did not alter body mass, adiposity, fasting blood glucose or serum insulin (Figure 3B–E). However, despite similar metabolic parameters the mice receiving feces from metformin-treated donors still had a dramatic reduction in tumor volume and tumor growth rate (Figure 3F,G)

comparable to the mice receiving metformin in the drinking water (Figure 2B). These data indicate that transplantation of the feces of HFD mice treated with metformin into metformin naïve mice fed a HFD, reduces tumor growth independently of differences in body mass, fasting blood glucose or insulin.

To interrogate whether the metformin-FMT reduced tumor growth through a mechanism involving changes in the gut microbiome we

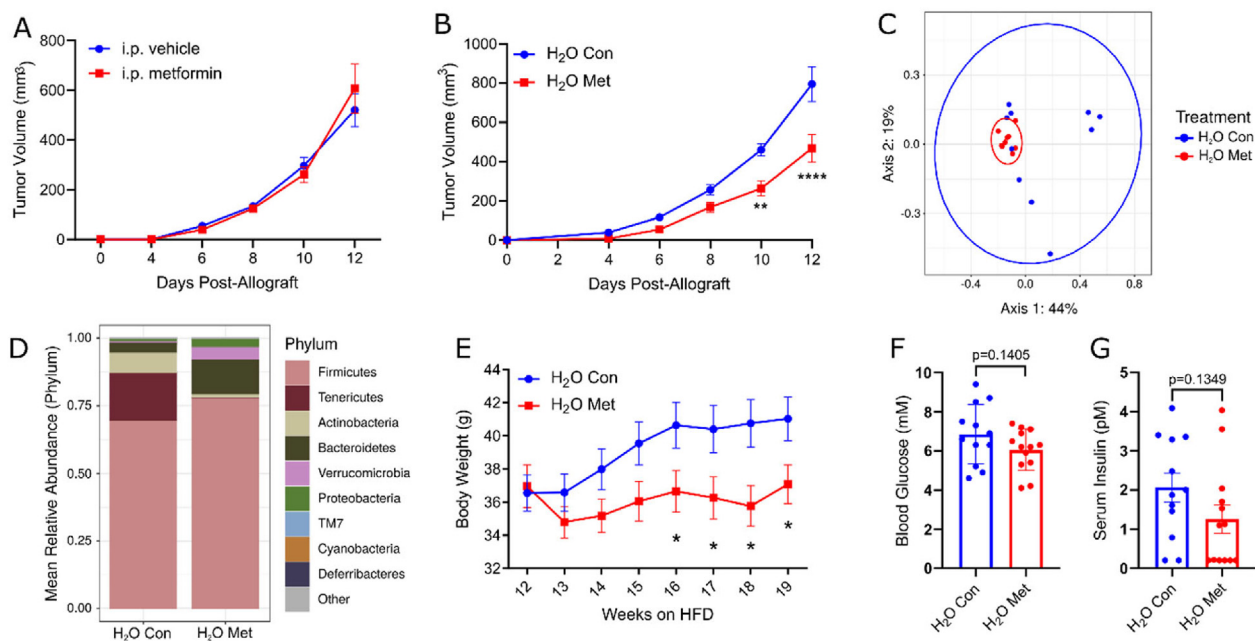


Figure 2: Oral metformin treatment changes the GMB, improves metabolic parameters and decreases MC38 tumor growth in HFD-fed mice. A) MC38 tumor allograft growth in HFD-fed mice treated with saline vehicle (i.p. vehicle, n = 18) or 100 mg/kg metformin (i.p. metformin, n = 18) by daily i.p. injection. B) MC38 tumor allograft growth in HFD-fed mice treated with control (H₂O Con, n = 12) or 250 mg/kg metformin delivered via drinking water (H₂O Met, n = 18). C) Principle coordinates of analysis of Bray–Curtis distances of 16S rRNA sequencing of fecal samples from mice treated with control (H₂O Con, n = 10) or 250 mg/kg metformin delivered via drinking water (H₂O Met, n = 9) supplemented water. D) Average relative abundances of fecal GMB phylum in mice drinking control (H₂O Con, n = 10) or 250 mg/kg metformin delivered via drinking water (H₂O Met, n = 9) supplemented water. E) Mouse body weight after 12-weeks of HFD-feeding and control (H₂O Con, n = 12) or 250 mg/kg metformin delivered via drinking water (H₂O Met, n = 13) treatment (starting on week 12 of HFD-feeding). F) 12-hour fasting blood glucose measurements in control (H₂O Con, n = 12) and 250 mg/kg metformin delivered via drinking water (H₂O Met, n = 13) mice. G) 12-hour fasting serum insulin levels in mice treated with control (H₂O Con, n = 12) or 250 mg/kg metformin delivered via drinking water (H₂O Met, n = 13) mice. Statistics: Unpaired two-sided t-testing (F, G), and repeated measures 2-way ANOVA (A, B, E) were used to test for differences between treatment groups with Sidak post-hoc testing. **p < 0.01, ****p < 0.0001.

removed live bacterial populations by sterile filtering feces before transplantation into donor mice. This process completely blocked metformin-FMT-mediated reductions in tumor growth, without altering body mass, fasting blood glucose or glucose tolerance (Figs. S3A–F). These data indicate that the inhibitory effect of metformin-treated feces on tumor growth was not due to residual metformin in the feces and requires live bacteria.

Given these findings we next sequenced the fecal microbiome and found that surprisingly, there were no major differences in β -diversity between HFD FMT and HFD-Met FMT mice (Figure 3H). However, linear discriminant analysis (LDA) identified 8 operational taxonomic units (OTUs) that with an increased abundance could distinguish between the treatment groups; one of which, *Alistipes* 72, was elevated in both metformin donor and HFD-Met FMT recipients (Figure 3I, Fig. S4). Five of the eight differential OTUs in the FMT mice belonged to the *Lachnospiraceae* or *Ruminococcaceae* families, which contain numerous SCFA-producing bacteria, which in addition to *Alistipes* may encode genes necessary for metabolizing lysine in butyrate synthesis [28,29]. Similarly, 10 of 27 enriched OTUs in the metformin-treated donor mice belonged to one of these two families. Otherwise, we did not detect differences in common CRC-associated bacteria, such as *Fusobacterium*, *Peptostreptococcus*, or *Porphyromonas*, in our differential abundance testing. These data indicate that the effects of orally delivered metformin on suppressing tumor growth can be in part recapitulated through transfer of the fecal microbiome and may involve increased abundance of SCFA-producing bacteria.

2.4. GMB-mediated anti-cancer effects of metformin act independent from GDF15 and tumor-infiltrating lymphocytes

We subsequently examined the potential mechanisms by which metformin induced modulation of the GMB might reduce tumor burden. Metformin increases serum concentrations of growth differentiating factor 15 (GDF15) [57] which has been linked to the suppression of appetite and improvements in glycemic control [58,59]. Increases in GDF15 have also been linked to reduced tumor growth [60] however, there was no difference in serum GDF15 between HFD-FMT and HFD-FMT-Met treated mice (58.42 \pm 3.12 pg/ml, n = 13 and 61.79 \pm 4.54 pg/ml, n = 15, respectively) suggesting this was unlikely the primary mechanism for the reduced tumor burden. Given the highly immunogenic nature of MC38 tumors [30] and the known connections between the GMB, immune function and T-cells in colorectal cancer [31] we hypothesized that metformin may be suppressing tumor growth by enhancing adaptive immunity as previously proposed [32]. Using flow cytometry (Fig. S5), we found that within the tumors of both HFD FMT and HFD-Met FMT mice there were no changes in markers of total T-cells, CD4+ T-cells, CD8+ T-cells, CD4+ T-cell proliferation (Ki67+) or T-cell activation (CD69+) (Figs. S6A–C). However, the use of cluster identification, characterization, and regression (Citrus) analysis (Figs. S6D and E), identified subtle differences between HFD FMT and HFD-Met FMT tumor immune cell infiltration. Specifically, HFD-Met FMT mice had a diminished population of highly activated cells expressing NK1.1 and Ki67 (Figs. S6F and G). This population displayed mixed expression of CD3 and CD8, suggesting a T cell population that has been recently exposed to antigen leading to down

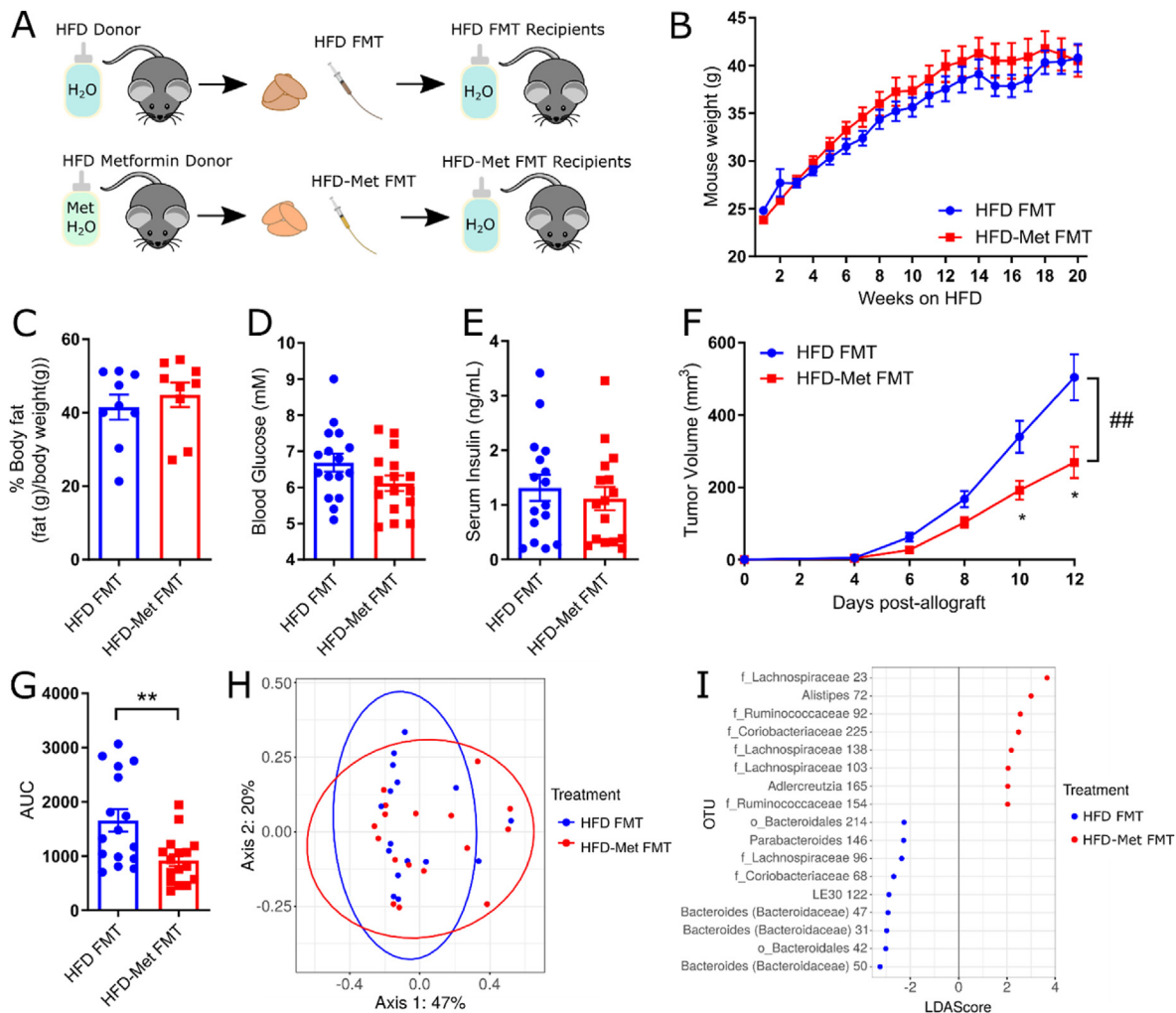


Figure 3: Fecal microbiome transfer from metformin-treated mice inhibits MC38 growth without changing metabolic parameters. A) Schematic depicting fecal microbiome transfer (FMT) from donor HFD-fed control mice or HFD-donor mice treated with 250 mg/kg metformin delivered via drinking water to HFD-fed FMT recipient animals. Donor and recipient mice were housed separately. 200 mL of fecal homogenate from donor mice were orally delivered to recipient mice 3 times weekly. B) Body weight in HFD ($n = 16$) and HFD-Met ($n = 16$) FMT recipient animals for the duration of their FMT protocol. C) Percent adiposity of HFD ($n = 9$) and HFD-Met ($n = 9$) FMT recipient animals, normalized to individual total body weight. D) 12-hour fasted blood glucose measurements in HFD ($n = 16$) and HFD-Met ($n = 16$) FMT recipient animals. E) 12-hour fasted serum insulin measurements in HFD ($n = 16$) and HFD-Met ($n = 16$) FMT recipient animals. F) MC38 tumor allograft growth in HFD ($n = 16$) and HFD-Met ($n = 16$) FMT recipient animals. G) Tumor growth rate in HFD ($n = 16$) and HFD-Met ($n = 16$) FMT recipient animals as calculated by the area under the curve of the MC38 tumor volume curve. H) Principle coordinates of analysis of Bray–Curtis distances of 16S rRNA sequencing of fecal samples from HFD-fed mice ($n = 16$) receiving FMT from control or metformin-treated HFD-fed ($n = 16$) donor mice. I) Linear discriminate analysis (LDA) of 16S rRNA sequencing of fecal material from HFD ($n = 16$) and HFD-Met ($n = 16$) FMT recipients, showing operational taxonomic units (OTU) associated with FMT from control (blue) or metformin (red) treated donor animals. Statistics: Repeated-measures 2-way ANOVA with Sidak post-hoc testing (B, F) and unpaired two-sided t-testing (C, D, E, G) was used to test for differences. * $p < 0.05$, ** $p < 0.01$, and ### $p < 0.01$ for overall treatment effect in 2-way ANOVA testing. (For interpretation of the references to color in this figure legend, the reader is referred to the Web version of this article.)

regulation of CD3 and CD8. Alternatively, these cells could reflect a mixed population of CD8+ T cells and NK cells. Curiously, these highly activated T-cells (NK1.1+, Ki67, cluster 79274) were correlated with tumor mass in HFD-FMT mice, suggesting a relationship between the presence of the cells and reduced tumor mass. However, this effect was not detected in HFD-Met FMT mice, suggesting that this population is not responsible for the growth suppression mediated by FMT from metformin-treated donors (Figs. S6H and I). Citrus analysis of a second independent panel of markers identified 4 clusters in which PD-1+ cells were significantly elevated in HFD-Met FMT tumors, which suggests, if anything, that T cell exhaustion may be elevated in tumors from mice treated by FMT from metformin-treated donors

(Fig. S6J). These data suggested that metformin fecal transfers were not inhibiting tumor growth by enhancing T cell activity within the tumor or disrupting the ratio of effector T cells to regulatory T cells.

2.5. SCFA production and tumor cholesterol metabolism gene expression are altered with GMB transfer from metformin-treated mice

This lack of significant changes in tumor infiltrating lymphocytes led us to hypothesize that metformin may be altering the production of bacterial-derived metabolites that might directly inhibit or stimulate tumor growth. To examine this possibility, we conducted serum metabolomics in mice receiving fecal transfers. HFD-fecal transfers

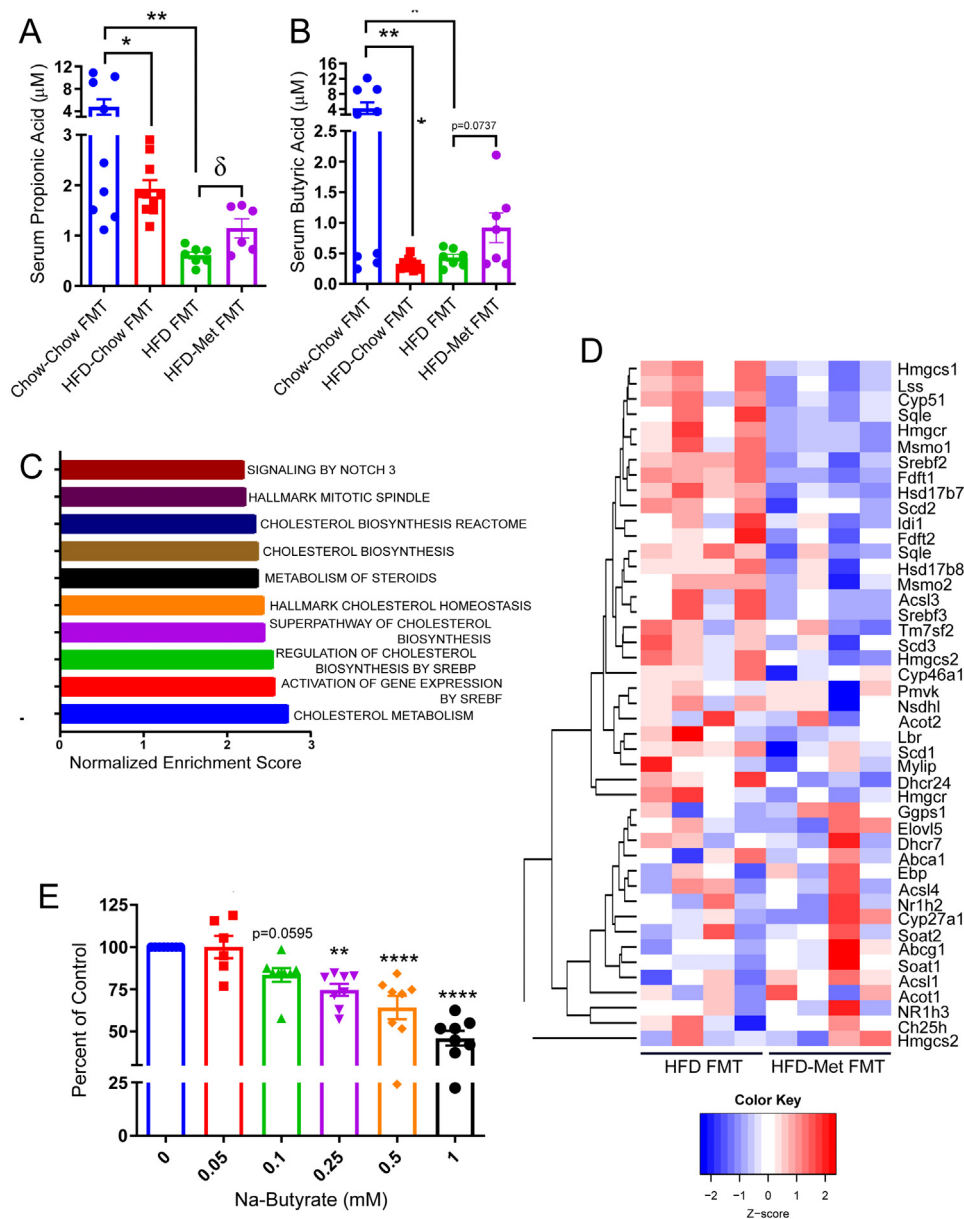


Figure 4: Fecal microbiome transfer affects short-chain fatty acid levels and changes the metabolic transcriptome of MC38 tumors in FMT recipient mice. A) Circulating propionic acid in serum in Chow–Chow (n = 9), HFD–Chow (n = 10), HFD (n = 7) and HFD–Met (n = 6) FMT recipient mice as measured by LC–MS. B) Circulating butyric acid in serum in Chow–Chow (n = 9), HFD–Chow (n = 10), HFD (n = 7) and HFD–Met (n = 6) FMT recipient mice as measured by LC–MS. C) Pathways identified with GSEA to have significant downregulation in HFD–Met FMT (n = 4) mice compared to HFD FMT (n = 4) mice. D) Heat map of genes in the cholesterol metabolism pathway (most enriched pathway in transcriptomics data set) (n = 4 per group). E) *In vitro* MC38 clonogenic growth with 0.05–1 mM of butyrate (n = 8 independent experiments for each concentration, excluding 0.05 mM, n = 6). Statistics: One-way ANOVA with Tukey (A, B, F) post-hoc testing, and unpaired two-sided t-testing (A, B, E) was used for a direct comparison of HFD–FMT and HFD–Met FMT (A, B). *p < 0.05, **p < 0.01, ****p < 0.0001; δ p < 0.05 for unpaired two-sided t-testing.

suppressed circulating levels of the SCFAs propionate and butyrate in chow fed mice consistent with previous findings [33,34] (Figure 4A,B). Importantly, these suppressive effects of the HFD were countered in metformin-treated donors which had increased levels of propionate (p = 0.0152) and a strong tendency for an increase in butyrate (p = 0.0737) compared to HFD FMT control animals (Figure 4A,B). There were no changes in other circulating fatty acids (Fig. S7). To examine potential mechanisms by which changes in the SCFAs of HFD–Met FMT mice inhibited tumor growth, we conducted global RNA-sequencing of the tumors. Using gene set enrichment analysis (GSEA) [35,36], we found that 815 gene sets were positively enriched in tumor

tissue from HFD–FMT mice as compared to HFD Met–FMT, 272 of which were significant at FDR < 25% (Fig. S8, Table S1). Conversely, 1098 gene sets were negatively enriched in tumor tissue from HFD–FMT mice compared to HFD Met–FMT tumors (Fig. S8, Table S1). Surprisingly, cholesterol metabolism and sterol response element binding protein (SREBP) gene targets dominated the list of gene sets that were significantly downregulated in HFD Met–FMT tumors (Table S1, Figure 4C,D). As cancer cells require cholesterol synthesis to support membrane biosynthesis for proliferation (reviewed in [37]) these data suggest that the fecal microbiome from metformin treated mice may suppress tumor growth by inhibiting cholesterol synthesis.

We next, cultured MC38 cells with metformin, propionate or butyrate. Consistent with previous studies in cultured MC38 cells [12], there was no inhibitory effect of clinically relevant concentrations of metformin on MC38 proliferation, except at concentrations >2 mM, which is outside the therapeutic window of exposure of <0.1 mM (Fig. S9). There was also no effect of propionate at concentrations <10 mM (Fig. S9). However, colony growth was dose-dependently decreased with butyrate treatment (Figure 4E). These data when combined with previous findings indicating butyrate suppresses transcription factors including SREBP and enzymes critical for cholesterol synthesis [43] suggest that metformin reduces tumor proliferation in HFD-fed mice by upregulating butyrate producing microbes.

3. DISCUSSION

The anti-cancer mechanisms of metformin treatment are complex and challenging to isolate. In the present work, we found that the GMB mediates metformin's effects against cancer using a murine model of CRC and fecal transfer protocols. This resulted in decreased tumor volume, increased SCFA levels in circulation, and a transcriptomic profile indicating reduced cholesterol metabolism. A strength of our experiments is that all fecal transfer experiments were completed into immunocompetent and fully colonized specific pathogen free (SPF) mice. Fecal microbiome transfers have been shown to transfer metformin treatment phenotypes from human samples into germ-free recipient animals [21,24]. While the use of germ-free mice is often required for studying human fecal effects, these models present inherent challenges that limit translation to human health and pathology. This includes impaired development of the immune system and intestinal tissue maturation, the inability of all human gut microbes to grow in the mouse intestinal tract, and the absence of environmental factors that human fecal donors are exposed to that are not recapitulated in the mouse environment [38]. Therefore, we sought to test the direct effects of metformin on the GMB by transferring feces from conventional HFD-fed, metformin-treated mice to HFD-fed conventional SPF mice. Thus, providing a model that is less intrinsically complicated that doesn't cross species and has an established baseline microbiome, fully developed immune system, and well-known metabolic phenotypes with HFD feeding. Using this model, we show that mice receiving an FMT from HFD-fed donor mice had alterations in their GMB and that this was associated with increased tumor growth. Treatment with oral, but not intraperitoneal, metformin decreased tumor growth in HFD-fed mice. FMT recipients of these HFD-Met fed mice also had reduced tumor growth, supporting a GMB-mediated mechanism.

Using 16S rRNA sequencing, we observed enrichment of OTUs belonging to the *Lachnospiraceae* and *Ruminococcaceae* families, which are SCFA producers [29], in the stool of both HFD-Met donor mice and their HFD-Met FMT recipient counterparts. SCFA producers, and specifically members of the *Lachnospiraceae* family, have also been reported to be decreased in CRC patients as compared to healthy volunteers [39]. We also identified that the OTU *Alistipes 72* was altered in both HFD-Met donor mice and HFD-Met FMT recipients, a phylum which may play a role in SCFA synthesis [28,29]. Indeed previous studies have found that *Alistipes* is elevated in HFD-fed metformin treated mice and is also correlated with improved glycemic control in metformin-treated patients with T2D [40]. However, notably, overall β -diversity was not significantly different between HFD-Met FMT mice and HFD FMT mice and in contrast to previous reports we found no change in glycemic parameters [40] with HFD-

fecal transfers. Considering the importance of the immune system to the GMB, the differences between studies could be due to our use of immune-competent animals. Remarkably, despite no change in parameters related to glycemic control we still observed reductions in tumor burden. To examine the potential mechanisms mediating the anti-tumor effects of the metformin GMB, we measured tumor infiltrating T cells and found no major difference in total levels of T-cells or their activation. However, Citrus analysis identified highly activated T-cell clusters (CD8+, NK1.1+, Ki67+) that were decreased in HFD-Met FMT tumors, an affect that could be linked to SCFA levels, with recent evidence showing butyrate can impact T-cell metabolism, decreasing Ki67 expression [41]. Subsequent, unbiased RNA-sequencing analysis identified marked suppression of genes critical for regulating cholesterol synthesis a process which is vital for supporting tumor cell proliferation (recently reviewed in [42]).

Our findings that the GMB from metformin treated mice and FMT recipients of those mice had increases in levels of SCFA producing bacteria are consistent with humans being treated with metformin [21,24]. They are also consistent with previous studies indicating butyrate inhibits colon cancer and suppresses transcription factors, including SREBP, and enzymes critical for cholesterol synthesis [30,43]. Thus these data strongly support a model where a GMB-butyrates axis is important for metformin-induced inhibition of tumor growth and suggest a mechanism by which diet and drugs interact to impact the GMB and influence carcinogenesis.

4. MATERIALS AND METHODS

4.1. Animal models and treatments

All experimental procedures and protocols were conducted in accordance with approval from the McMaster Animal Research Ethics Board. 6-week old C57BL/6J mice (Jackson Laboratories, Bar Harbour, ME, USA) were fed standard chow (17% kcal from fat; Diet 8640, Harlan Teklad) or 45% high-fat diet (HFD; D12451, Research Diets, Cedarlane) *ad libitum*. After 12 weeks of HFD-feeding, animals were weight matched into groups before commencement of treatments. Metformin administration was via daily i.p. injections (100 mg/kg body weight), or in drinking water (250 mg/kg body weight adjusted to weights weekly, refreshed 3x weekly, and stored at 4 °C until use). Mice were maintained on a 12-hour light/dark schedule, with ambient room temperatures of 23–24 °C, bedding and enrichment, and *ad libitum* access to drinking water. Body weights were measured weekly. Total adipose, lean, and liquid mass was measured using a time-domain NMR whole-body composition analyser (Minispec LF90II, Bruker, Milton, ON) with the Minispec Plus and Opus programs (Bruker, Milton, ON). Percent body fat was calculated as g adipose/g bodyweight (measured at time of scan) * 100.

4.2. Metabolic testing and measurements

Mice were fasted for 6h following the dark/feeding cycle. Mouse weights and baseline blood glucose measurements were taken with a commercial glucometer (Aviva, Roche), and mice were i.p. injected with 1 g/kg bodyweight of glucose. Blood glucose measurements were taken at 20, 40, 60, 90, and 120 min after glucose injection. Fasting blood glucose was taken using commercial glucometers (Aviva, Roche) following an overnight, 12-hour fast. Blood was collected after this fast and serum insulin was measured by ELISA (Millipore). Blood samples were allowed to clot at room temperature for 30 min, centrifuged at 14,000rpm for 10 min at 4 °C, and stored at –80 °C until use. ELISA data was analyzed by curve fitting of the output data and was

Brief Communication

conducted with 4-parameter logistic regression analysis on free software available at elisaanalysis.com.

4.3. MC38 tumor allograft model

MC38 murine colon cancer cells (provided by Dr. Michael Pollak, McGill University, Montreal, Canada) were maintained in DMEM (Gibco) media with 10% fetal bovine serum (Gibco) and 1% anti-anti solution (Gibco). Cells were maintained in an incubator at 37 °C and 5% CO₂. Mice were anaesthetized using isoflurane, shaved on their hind flank with an electric razor, and injected with 5×10^5 cells in 100 μL warm PBS. A 25G needle was used for injections to avoid disrupting cells during injection. When tumors were palpable (3–4 days post-injection), tumor volume measurements were conducted every other day using a Vernier hand caliper. Tumor volume was calculated using the formula $V = 0.5(\text{length} * \text{width}^2)$.

4.4. Fecal microbiome and fecal filtrate transfer protocol

Recipient cages ($n = 2-3$ per cage) corresponded to specific donor cages ($n = 2-3$ per cage) and recipients and donors were matched for the duration of the experiment (no mixing of donor/recipient cages after protocol start). Donor animals were on control or metformin-supplemented water for 24-hours prior to fecal transfer initiation. Feces were collected from donor cages prior to dilution (1:10 wt/vol) in 0.9% saline solution. Feces and saline were combined in conical tubes and vortexed until homogenous (approximately 5 min, maximum vortex speed), and centrifuged for 30 s at 2000rpm, and the supernatant collected. Fecal filtrates were produced by filtering the supernatant sequentially through sterile syringe filters (0.45 μm and 0.22 μm, MilliporeSigma). 200 μL of the resulting supernatant and filtrate was gavaged into recipient mice 3 times weekly for the remaining duration of the study.

4.5. Cell culture proliferation and clonogenic assays

MC38 cells were grown in 25 mM glucose DMEM or 5 mM glucose DMEM for two weeks prior to seeding. Metformin (Sigma Aldrich) and sodium (Na-)butyrate (Sigma Aldrich), and sodium (Na-)propionate (Sigma Aldrich) were made fresh prior to each experiment, and were solubilized into water for treatments. Proliferation assays were conducted by plating 500–1000 cells/well in 96-well plates with fecal filtrate (prepared in supplemented DMEM following the protocol above) at a maximum concentration of 25%, and serially diluted. Cells grew for 72 h, and were stained with 0.5% crystal violet stain (Sigma Aldrich) in 40% ethanol, washed in water, and allowed to dry overnight. Remaining dye was dissolved in 0.5M NaH₂PO₄ (Sigma Aldrich) solution and read at 570 nm on a plate reader. For clonogenic assays, 200 cells per well were seeded into 12-well plates, and allowed to adhere overnight. Treatments were applied in triplicate the following day, and cultures were monitored daily. Once cells had proliferated and produced colonies (approximately 5–7 days), cells were washed with PBS and stained with 0.5% crystal violet stain in 40% ethanol (Sigma Aldrich). Once dried, colonies containing more than 50 cells were counted using a grid mounted under the 12-well plate to ensure accuracy.

4.6. 16S rRNA sequencing

Fresh fecal samples were collected between 7 and 9AM on the day prior to sacrifice. Fecal pellets were stored in autoclaved tubes at –80 °C. A commercially available kit was used for DNA extraction (Zymo Research, Cat. No D6012). 16S rRNA amplification and sequencing was conducted in the McMaster Farncombe Institute Genomics Facility. Purified DNA was used to amplify the v3 region of the

16S rRNA gene by PCR. 50 ng of DNA was used as template with 1U of Taq, 1x buffer, 1.5 mM MgCl₂, 0.4 mg/mL BSA, 0.2 mM dNTPs, and 5 pmol each of 341F (CCTACGGGAGGAGCAG) and 518R (ATTACCGCGGCTGCTGG) Illumina adapted primers, as described in Bartram et al. (2011) [46]. The reaction was carried out at 94 °C for 5 min, 25 cycles of 94 °C for 30 s, 50 °C for 30 s and 72 °C for 30 s, with a final extension of 72 °C for 10 min. Resulting PCR products were visualized on a 1.5% agarose gel. Positive amplicons were normalized using the SequalPrep normalization kit (ThermoFisher#A1051001) and sequenced on the Illumina MiSeq platform at the McMaster Genomics Facility. Resulting sequences were run through the sl1p pipeline as described in Whelan et al. (2017) [47].

4.7. Analysis of 16S rRNA sequencing

All microbiome analysis was conducted in R (version 3.4.4) [48]. Data were curated using the phyloseq package (version 1.22.3) [49] and all microbiome figures were plotted using ggplot2 (version 3.0.0) [50]. OTUs were filtered to remove all non-bacterial reads and any OTUs present only once in the data set. Bray–Curtis distances were calculated using the distance() function in phyloseq, and PCoA plots were generated using phyloseq and ggplot2. To generate taxa bar charts, data were organized using the following tidyverse [51] packages: dplyr (version 0.7.6), tidyr (0.8.1), and rlang (0.2.0). The plots were generated using ggplot2. Color palettes used in the figures came from the RColorBrewer package (1.1.2) [52]. PERMANOVA tests were conducted using the vegan package (2.5.2). Exploratory analysis of OTUs contributing to the separation of metformin-treated and control mice was conducted using LEfSe [53] with all default parameters. Linear models of Shannon and Simpson diversity were fit using lm() in R.

4.8. Quantitation of serum lipids

Quantitation of fatty acids was performed using 3-NPH derivatization – UPLC-MRM/MS according to the procedures previously published [54]. Briefly, 20 μL of the supernatant of each serum sample was mixed with 280 μL of methanol. The mixture was vortex-mixed and sonicated in an ice-water bath for 5 min, followed by centrifugal clarification. 100 μL of the supernatant was mixed with 50 μL of 150-mM 3-NPH solution and 50-μL of 100-mM EDC.HCl-6% pyridine solution. The mixtures were allowed to react at 35 °C for 40 min in a thermomixer at a shaking frequency of 900 rpm. After the reaction, 50 μL of an internal standard solution containing the ¹³C₆-3-NPH derivatives of all the targeted fatty acids, which were prepared in a “one-pot” reaction with the use of the standard substances of fatty acids was added. After mixing, 10 μL was injected onto a Waters BEH C18 column (2.1 mm I.D. x 50 mm, 1.7 μm) for LC separation with a mobile phase composed of (A) 0.01% formic acid in water and (B) 0.01% formic acid in isopropanol for binary-solvent gradient elution. Concentrations of short-, medium and long-chain fatty acids in each sample were calculated from the standard curves of the individual analytes with internal-standard calibration. The calibration curves were prepared in parallel with the sample analyses using serially diluted, mixed standard solutions of individual fatty acids. An Agilent 1290 UHPLC system coupled to an Agilent 6495B QQQ mass spectrometer equipped with an electrospray ion (ESI) source was used. This MS instrument was operated in the multiple-reaction monitoring (MRM) mode with negative-ion (–) detection for analysis of fatty acids.

4.9. RNA sequencing and transcriptomics

RNA was isolated from frozen tumor samples maintained at –80 °C using TRIzol reagent (Invitrogen, CA, USA) and purified in columns

(RNeasy kit; Qiagen, CA, USA). Sequencing was conducted at the McMaster Genomics Facility, Farncombe Institute at McMaster University. Sample quality was first assessed using a bioanalyzer (Agilent 2100 Bioanalyzer G2938C, Agilent RNA 6000 Nano Kit, Agilent; Santa Clara, CA, USA), then enriched (NEBNext Poly(A) mRNA Magnetic Isolation Module; NEB, Ipswich, MA, USA). Library preparations were conducted (NEBNext Ultra II Directional RNA Library Prep Kit; NEB, Ipswich, MA, USA) and library fragment size distribution was verified (Agilent TapeStation D1000; Agilent, Santa Clara, CA, USA). Libraries were quantified by qPCR, pooled in equimolar amounts, and qPCR and fragment size distribution verification was conducted again. Libraries were then sequenced on an Illumina HiSeq 1500 across 2 lanes of a HiSeq Rapid v2 flow cell (Illumina; San Diego, CA, USA) using a paired-end, 2×51 bp configuration, with onboard cluster generation. All supplier-provided protocols were followed. FastQC (<https://www.bioinformatics.babraham.ac.uk/projects/fastqc/>) was used to test for sequence quality and low-quality reads were removed with Trimmomatic10 (using default parameters). Reads were aligned to Ensembl *Mus musculus* (GRCm38.92) genome using HISAT211 (default parameters). htseq-count identified the number of reads that mapped to each gene (advanced options used: stranded set to “reverse”, minimum alignment quality set to 10, feature type set to “exon” and “simple”). Ensembl mouse GTF gene annotation was used. Default parameters of DESeq212 normalized data and a custom python script (McArthur) converted the DESeq2 output into a ranked list of genes. Gene Set Enrichment Analysis (GSEA) [35,36] was performed on the ranked list of genes using 1000 permutations, a 25% false-discovery rate, and mouse gene set data base (Bader Lab, University of Toronto, http://download.baderlab.org/EM_Genesets/current_release/Mouse). Gene enrichment map was made using Cytoscape 3.7.2 to visualize pathways, with Q-value cut off of 0.02, and edge cut-off of 0.5. Heatmaps were generated in R using the heatmap.2 function from the gplots package (version 3.0.3). Log-transformed normalized counts for cholesterol related genes were scaled by row based on the z-score and clustered using the hclust() and dist() functions.

4.10. T-cell profiling using flow cytometry

Fresh tumor samples were collected from mice, and mechanically homogenized by hand in a prepared digest solution containing HyClone Hank's balanced salt solution (ThermoFisher; Waltham, MA, USA), 0.5 mg/mL collagenase type I (isolated from *Clostridium histolyticum*, ThermoFisher/Gibco, Waltham, MA, USA) and 0.2 mg/mL DNaseI (from Bovine pancreas, MilliporeSigma, Burlington, MA, USA). Homogenates digested for 1h at 37 °C, rotating at 200rpm, then consecutively strained through 70 μ m and 40 μ m nylon cell strainers (ThermoFisher; Waltham, MA, USA). Homogenates were pelleted for 5 min at 1500rpm, and resuspended in ACK buffer (0.15M NH₄Cl, 10 mM KHCO₃) for 5 min at room temperature to lyse red blood cells in the samples. ACK lysis was stopped with ice cold PBS, samples pelleted, and ACK lysis was repeated. Resulting pellets were resuspended in cold PBS for cell counting and staining. Fluorescent antibody staining was conducted in a 96-well round-bottom plate containing 1×10^6 cells/well. Briefly, cells were stained with NEAR IR Live/Dead stain (1:1000 dilution in PBS; ThermoFisher; Waltham, MA, USA) following manufacturer's protocol. Blocking was conducted with Fc Block (1:200 in PBS with 0.5% w/v BSA) for 15 min on ice. Antibodies for surface markers were applied with the dilutions provided in the table below. Intracellular markers were fixed and permeabilized (FOXP3/Transcription factor staining buffer set, eBioscience/ThermoFisher, CA, USA), then stained with fluorescent antibodies. Counting beads (123count eBeads, ThermoFisher; Waltham, MA, USA) were used to

quantify cell numbers. To prepare for flow cytometry, samples were resuspended in 200 μ L of PBS with 0.5% w/v BSA, and filtered through nylon mesh into FACS tubes. Samples were run on BD LSRFortessa. Data were analyzed on FlowJo version 10.6.0, with gate setting guided by lymphocytes isolated from fresh spleens, or spleen-isolated lymphocytes that were stimulated or unstimulated.

Panel	Component	Supplier	Cat No	Lot No	Dilution
Core Panel	CD45.2 BV510	BioLegend	109838	B266852	1:25
	CD3 BV605	BD	563004	9137680	1:50
	CD4 PerCP-Cy5.5	BD	550954	8346562	1:100
	CD8 AF700	BD	557959	9025745	1:100
Panel 1	CD25 BV711	BioLegend	102049	B282102	1:400
	NK1.1 PE-CF594	BD	562864	8318558	1:100
	CD69 APC	BioLegend	104514	B247009	1:40
	KLRG1 AF488	BD	561619	7306667	1:20
	FOXP3 PE	eBioscience	12-5773-82	2001196	1:160
Panel 2	Ki67 BV421	BioLegend	652411	B265335	1:150
	CD44 AF488	BioLegend	103016	B234375	1:50
	CD62L PE-Cy7	BioLegend	104418	B269976	1:200
	PD1 BV421	BD	562584	9014528	1:40
	CTLA4 PE	BioLegend	106306	B251635	1:40
CD27 BV785	BioLegend	124241	B283652	1:100	

4.11. CITRUS methodology

Using a semi-supervised machine learning approach called CITRUS (cluster identification, characterization, and regression), we sought to identify features that differentiated the HFD-FMT and HFD Met-FMT groups. CITRUS [55] can characterize clusters of significance using a variety of metrics which are calculated on a per-sample basis. Panels 1 and 2 were analysed by CITRUS using metrics that suited each individually. To minimize noise, our analysis for both panels included only live CD45+ single cells (“cells”), pre-processed in FlowJo v.10.6.2 (Becton Dickinson). CITRUS was run using RStudio v.1.2.5042 (RStudio, Inc.) running R v.3.6.3 (r-project.org). Cells were down-sampled to equal sizes for each sample. Clusters were limited to a minimum of 2% of total cells. HFD-FMT and HFD Met-FMT sample groups were compared in a pairwise manner. Cells were concatenated from samples within the two groups. After unsupervised agglomerative hierarchical clustering with chosen markers, cluster abundances or median fluorescence intensities of chosen markers were input into a nearest-shrunken centroid regression model (PAMR) to determine if the differences between groups was significant [56]. Panel 1 clustering was performed using 5,000 down-sampled cells from each sample with the following markers: CD3, CD4, CD8, CD25, CD69, FoxP3, Ki-67, KLRG1 and NK1.1. Abundance features were used to quantify the proportion of a sample's cells that belong to a cluster. Panel 2 clustering was performed using 10,000 down-sampled cells from each sample with the following markers: CD3, CD4, CD8, CD27, CD44 and CD62L. Median features were used to quantify the median fluorescence intensity (MFI) value of the following functional markers in a cluster's cells: PD-1 and CTLA4. Antibodies are as listed above.

4.12. Statistical analysis

Unless stated otherwise, all data is presented as mean with SEM. Data were analyzed and plotted in GraphPad Prism 8, except for 16S rRNA and RNA sequencing analysis, which were analyzed as described above. Depending on experimental design, two-sided t-tests, 1-way and 2-way ANOVA were used to test for significant variation, with post-hoc testing as documented in figure legends to test for differences between groups. Simple linear regression was used for linear

curve fitting with R^2 and 95% confidence intervals presented on the figure. Significance was determined at $p < 0.05$. Graphical abstract was generated using biorender.com.

AUTHOR CONTRIBUTIONS

L.A.B., G.R.S., and J.D.S. designed the experiments. L.A.B., A.S., J.A.H., K.S., J.G., and M.J.B. performed experiments and contributed to data analysis. J.C.S., J.M., J.W., A.R.R., and A.S. provided bioinformatics analysis and visualization support. LAB and GRS wrote the manuscript. All authors edited the manuscript and provided comments.

DATA AVAILABILITY

Data is not currently available on a public repository. All reasonable requests for raw data will be considered upon request of G.R.S.

ACKNOWLEDGEMENTS

Authors would like to thank Dr. Jun Han of the University of Victoria Genome BC Proteomics center, a node of The Metabolomics Innovation Centre (TMIC) for metabolomics measurements. G.R.S. is a Canada Research Chair and the J. Bruce Duncan Chair in Metabolic Diseases. This study was supported by research grants from the Canadian Cancer Society, Canadian Institutes of Health Research (201709FDN-CEBA-116200 and 144625-1 to GRS) and Diabetes Canada (DI-5-17-5302-GS).

CONFLICT OF INTEREST

The authors declare no conflicts of interest related to the findings described in this manuscript.

APPENDIX A. SUPPLEMENTARY DATA

Supplementary data to this article can be found online at <https://doi.org/10.1016/j.molmet.2022.101498>.

REFERENCES

- [1] Kyrgiou, M., Kalliala, I., Markozannes, G., Gunter, M., Paraskevidis, E., Gabra, H., et al., 2017. Adiposity and cancer at major anatomical sites: umbrella review of the literature. *BMJ* 356:1–10.
- [2] Dong, Y., Zhou, J., Zhu, Y., Luo, L., He, T., Hu, H., et al., 2017. Abdominal obesity and colorectal cancer risk: systematic review and meta-analysis of prospective studies. *Bioscience Reports* 37. BSR20170945.
- [3] González, N., Prieto, I., Del Puerto-Navado, L., Portal-Núñez, S., Antonio Ardura, J., Corton, M., et al., 2017. Update on the relationship between diabetes and colorectal cancer: epidemiology, potential molecular mechanisms and therapeutic implications. *Oncotarget* 8:18456–18485, 2017.
- [4] Ma, Y., Yang, W., Song, M., Smith-Warner, S., Yang, J., Li, Y., et al., 2018. Type 2 diabetes and risk of colorectal cancer in two large U.S. prospective cohorts. *British Journal of Cancer* 119:1436–1442.
- [5] Ulrich, C.M., Himbert, C., Holowatyj, A.N., Hursting, S.D., 2018. Energy balance and gastrointestinal cancer: risk, interventions, outcomes and mechanisms. *Nature Reviews Gastroenterology & Hepatology* 15:683–698.
- [6] Kilil-Drori, A.J., Azoulay, L., Pollak, M.N., 2017. Cancer, obesity, diabetes, and antidiabetic drugs: is the fog clearing? *Nature Reviews Clinical Oncology* 14: 85–99.
- [7] Garber, A.J., Abrahamson, M., Barzilay, J., Blonde, L., Bloomgarden, Z., Bush, M., et al., 2015. AACE/ACE comprehensive diabetes management algorithm. *Endocrine Practice* 21:438–447, 2015.
- [8] Pollak, M., 2013. Potential applications for biguanides in oncology. *Journal of Clinical Investigation* 123:3696–3700.
- [9] Dowling, R.J.O., Goodwin, P.J., Stambolic, V., 2011. Understanding the benefit of metformin use in cancer treatment. *BMC Medicine* 9:33.
- [10] Pernicova, I., Korbonits, M., 2014. Metformin-mode of action and clinical implications for diabetes and cancer. *Nature Reviews Endocrinology*. <https://doi.org/10.1038/nrendo.2013.256>.
- [11] Algire, C., Amrein, L., Zakikhani, M., Panasci, L., Pollak, M., 2010. Metformin blocks the stimulative effect of a high-energy diet on colon carcinoma growth in vivo and is associated with reduced expression of fatty acid synthase. *Endocrine-Related Cancer* 17:351–360.
- [12] Algire, C., Amrein, L., Bazile, M., David, S., Zakikhani, M., Pollak, M., et al., 2011. Diet and tumor LKB1 expression interact to determine sensitivity to anti-neoplastic effects of metformin in vivo. *Oncogene* 30:1174–1182.
- [13] Qin, J., Li, Y., Cai, Z., Li, S., Zhu, J., Zhang, F., et al., 2012. A metagenome-wide association study of gut microbiota in type 2 diabetes. *Nature* 490:55–60.
- [14] Karlsson, F.H., Tremaroli, V., Nookaew, I., Bergstrom, G., Behre, C., Fagerberg, B., et al., 2013. Gut metagenome in European women with normal, impaired and diabetic glucose control. *Nature* 498:99–103.
- [15] Vogtmann, E., Hua, X., Zeller, G., Sunagawa, S., Voigt, A., Hercog, R., et al., 2016. Colorectal cancer and the human gut microbiome: reproducibility with whole-genome shotgun sequencing. *PLoS One* 11:1–13.
- [16] Feng, Q., Liang, S., Jia, H., Stadlmayr, A., Tang, L., Lan, Z., et al., 2015. Gut microbiome development along the colorectal adenoma–carcinoma sequence. *Nature Communications* 6:6528.
- [17] Ohgashi, S., Sudo, K., Kobayashi, D., Takahashi, O., Takahashi, T., Asahara, T., et al., 2013. Changes of the intestinal microbiota, short chain fatty acids, and fecal pH in patients with colorectal cancer. *Digestive Diseases and Sciences* 58:1717–1726.
- [18] De Vadder, F., Kovatcheva-Datchary, P., Goncalves, D., Vinera, J., Zitoun, C., Duchamp, A., et al., 2014. Microbiota-generated metabolites promote metabolic benefits via gut-brain neural circuits. *Cell* 156:84–96.
- [19] Wang, J., Jia, H., 2016. Metagenome-wide association studies: fine-mining the microbiome. *Nat Rev Microbiol* Accepted i, 508–522.
- [20] Ocvirk, S., Wilson, A.S., Appolonia, C.N., Thomas, T.K., O’Keefe, S.J.D., 2019. Fiber, fat, and colorectal cancer: new insight into modifiable dietary risk factors. *Current Gastroenterology Reports* 21.
- [21] Forslund, K., Hildebrand, F., Nielsen, T., Falony, G., 2015. Disentangling the effects of type 2 diabetes and metformin on the human gut microbiota. *Nature* 528:262–266.
- [22] Shin, N.-R., Lee, J.-C., Lee, H.-Y., Kim, M.-S., Whon, T., Lee, M.-S., et al., 2014. An increase in the Akkermansia spp. population induced by metformin treatment improves glucose homeostasis in diet-induced obese mice. *Gut* 63: 727–735.
- [23] De La Cuesta-Zuluaga, J., Mueller, N., Corrales-Agudelo, V., Velasquez-Mejia, E., Carmona, J., Abad, J., et al., 2017. Metformin is associated with higher relative abundance of mucin-degrading akkermansia muciniphila and several short-chain fatty acid-producing microbiota in the gut. *Diabetes Care* 40:54–62.
- [24] Wu, H., Esteve, E., Tremaroli, V., Khan, M., Caesar, R., Mannerholm, L., et al., 2017. Metformin alters the gut microbiome of individuals with treatment-naive type 2 diabetes, contributing to the therapeutic effects of the drug. *Nature Medicine* 23:850–858.
- [25] Bauer, P.V., Duca, F., Waise, T., Rasmussen, B., Abraham, M., Dranse, H., et al., 2018. Metformin alters upper small intestinal microbiota that impact a glucose-SGLT1-sensing glucose regulatory pathway. *Cell Metabolism* 27:101–117 e5.
- [26] Dowling, R.J.O., Lam, S., Bassi, C., Mouaaz, S., Aman, A., Kiyota, T., et al., 2016. Metformin pharmacokinetics in mouse tumors: implications for human therapy. *Cell Metabolism* 23:567–568.
- [27] Chandel, N.S., Avizonis, D., Reczek, C., Weinberg, S., Menz, S., Christian, S., et al., 2016. Are metformin doses used in murine cancer models clinically relevant? *Cell Metabolism* 23:569–570.

- [28] Vital, M., Howe, A., Tiedje, J., 2014. Revealing the bacterial synthesis pathways by analyzing (meta) genomic data. *mBio* 5:e00889.
- [29] Vital, M., Karch, A., Pieper, D.H., 2017. Colonic butyrate-producing communities in humans: an overview using omics data. *mSystems* 2 e00130-17.
- [30] Efremova, M., Rieder, D., Klepsch, V., Charoentong, P., Finotello, F., Hackl, H., et al., 2018. Targeting immune checkpoints potentiates immunoeediting and changes the dynamics of tumor evolution. *Nature Communications* 9.
- [31] Angelova, M., Charoentong, P., Hackl, H., Fischer, M., Snajder, R., Krogsdam, A., et al., 2015. Characterization of the immunophenotypes and antigenomes of colorectal cancers reveals distinct tumor escape mechanisms and novel targets for immunotherapy. *Genome Biology* 16:1–17.
- [32] Cha, J.H., Yank, W.-H., Xia, W., Wei, Y., Chan, L.-C., Lim, S.-O., et al., 2018. Metformin promotes antitumor immunity via endoplasmic-reticulum-associated degradation of PD-L1. *Molecular Cell* 71:606–620 e7.
- [33] Jakobsdottir, G., Xu, J., Molin, G., Ahrné, S., Nyman, M., 2013. High-fat diet reduces the formation of butyrate, but increases succinate, inflammation, liver fat and cholesterol in rats, while dietary fibre counteracts these effects. *PLoS One* 8:1–15.
- [34] Topping, D.L., Clifton, P.M., 2001. Short-chain fatty acids and human colonic function: roles of resistant starch and nonstarch polysaccharides. *Physiological Reviews* 81:1031–1064.
- [35] Mootha, V.K., Lindgren, C., Eriksson, K.-F., Subramanian, A., Sihag, S., Lehar, J., et al., 2003. PGC-1 α -responsive genes involved in oxidative phosphorylation are coordinately downregulated in human diabetes. *Nature Genetics* 34:267–273.
- [36] Subramanian, A., Tamayo, P., Mootha, V., Sayan, M., Ebert, B., Gillette, M., et al., 2005. Gene set enrichment analysis: a knowledge-based approach for interpreting genome-wide expression profiles. *Proceedings of the National Academy of Sciences* 102:15545–15550.
- [37] Zhang, C., Yue, C., Herrmann, A., Song, J., Egelston, C., Wang, T., et al., 2020. STAT3 activation-induced fatty acid oxidation in CD8 + T effector cells is critical for obesity- promoted breast tumor growth. *Cell Metabolism* 31:1–14.
- [38] Walter, J., Armet, A.M., Finlay, B.B., Shanahan, F., 2020. Establishing or exaggerating causality for the gut microbiome: lessons from human microbiota-associated rodents. *Cell* 180:221–232.
- [39] Flemer, B., Lynch, D., Brown, J., Jeffrey, I., Ryan, R., Claesson, M., et al., 2017. Tumour-associated and non-tumour-associated microbiota in colorectal cancer. *Gut* 66:633–643.
- [40] Lee, H., Ko, G., 2014. Effect of metformin on metabolic improvement and gut microbiota. *Applied and Environmental Microbiology* 80:5935–5943.
- [41] Bachem, A., Makhlof, C., Binger, K., de Souza, D., Tull, D., Hochheiser, K., et al., 2019. Microbiota-derived short-chain fatty acids promote the memory potential of antigen-activated CD8+ T cells. *Immunity* 51:285–297 e5.
- [42] Ding, X., Zhang, W., Li, S., Yang, H., 2019. The role of cholesterol metabolism in cancer. *Am. J. Cancer Res.* 9:219–227.
- [43] Alvaro, A., Sola, R., Rosales, R., Ribalta, J., Anguera, A., Masana, L., et al., 2008. Gene expression analysis of a human enterocyte cell line reveals downregulation of cholesterol biosynthesis in response to short-chain fatty acids. *IUBMB Life* 60:757–764.
- [46] Bartram, A.K., Lynch, M.D.J., Stearns, J.C., Moreno-Hagelsieb, G., Neufeld, J.D., 2011. Generation of multimillion-sequence 16S rRNA gene libraries from complex microbial communities by assembling paired-end Illumina reads. *Applied and Environmental Microbiology* 77: 3846–3852.
- [47] Whelan, F.J., Surette, M.G., 2017. A comprehensive evaluation of the sl1p pipeline for 16S rRNA gene sequencing analysis. *Microbiome* 5:1–13.
- [48] R Core Team. R, 2013. A language and environment for statistical Computing. Vienna, Austria: R Foundation for Statistical Computing. Available at: <https://www.r-project.org/>. (Accessed 29 July 2018).
- [49] McMurdie, P.J., Holmes, S., 2013. Phyloseq: an R package for reproducible interactive analysis and graphics of microbiome census data. *PLoS One* 8: e61217.
- [50] Gómez-Rubio, V., 2017. ggplot2 - elegant graphics for data analysis (2nd edition). *Journal of Statistical Software* 77:3–5.
- [51] Wickham, H., 2017. Tidyverse packages - tidyverse. Available at: <https://www.tidyverse.org/packages/>. (Accessed 29 July 2018).
- [52] Neuwirth, E., 2014. RColorBrewer: ColorBrewer palettes. Available at: <https://cran.r-project.org/web/packages/RColorBrewer/index.html>. (Accessed 29 July 2018).
- [53] Segata, N., Izard, J., Waldron, L., Gevers, D., Miropolsky, L., Garrett, W., et al., 2011. Metagenomic biomarker discovery and explanation. *Genome Biology* 12.
- [54] Han, J., Lin, K., Sequeira, C., Borchert, C.H., 2015. An isotope-labeled chemical derivatization method for the quantitation of short-chain fatty acids in human feces by liquid chromatography-tandem mass spectrometry. *Analytica Chimica Acta* 854:86–94.
- [55] Bruggner, R.V., Bodenmiller, B., Dill, D.L., Tibshirani, R.J., Nolan, G.P., 2014. Automated identification of stratifying signatures in cellular subpopulations. *Proceedings of the National Academy of Sciences of the United States of America* 111.
- [56] Tibshirani, R., Hastie, T., Narasimhan, B., Chu, G., 2002. Diagnosis of multiple cancer types by shrunken centroids of gene expression. *Proceedings of the National Academy of Sciences of the United States of America* 99:6567–6572.
- [57] Gerstein, H.C., et al., 2017. Growth Differentiation Factor 15 as a Novel Biomarker for Metformin. *Diabetes Care* 40(2):280–283. <https://doi.org/10.2337/dc16-1682>.
- [58] Coll, A.P., et al., 2020. GDF15 mediates the effects of metformin on body weight and energy balance. *Nature* 578(7795):444–448. <https://doi.org/10.1038/s41586-019-1911-y>.
- [59] Day, E.A., 2019. Metformin-induced increases in GDF15 are important for suppressing appetite and promoting weight loss. *Nature Metabolism* 1(12): 1202–1208. <https://doi.org/10.1038/s42255-019-0146-4>.
- [60] Husaini, Y., et al., 2020. Growth differentiation factor-15 slows the growth of murine prostate cancer by stimulating tumor immunity. *PLoS One* 15(6): e0233846. <https://doi.org/10.1371/journal.pone.0233846>.